Two-dimensional nanolithography using atom interferometry

A. Gangat, P. Pradhan, G. Pati, and M. S. Shahriar
Department of Electrical and Computer Engineering, Northwestern University, Evanston, Illinois 60208, USA
(Received 4 May 2004; published 12 April 2005)

We propose a scheme for the lithography of arbitrary, two-dimensional nanostructures via matter-wave interference. The required quantum control is provided by a $\pi/2$-π-$\pi/2$ atom interferometer with an integrated atom lens system. The lens system is developed such that it allows simultaneous control over the atomic wave-packet spatial extent, trajectory, and phase signature. We demonstrate arbitrary pattern formations with two-dimensional ^{87}Rb wave packets through numerical simulations of the scheme in a practical parameter space. Prospects for experimental realizations of the lithography scheme are also discussed.

DOI: 10.1103/PhysRevA.71.043606 PACS number(s): 03.75.Dg, 39.20.+q, 04.80.−y, 32.80.Pj

I. INTRODUCTION

The last few decades have seen a great deal of increased activity toward the development of a broad array of lithographic techniques [1,2]. This is because of their fundamental relevance across all technological platforms. These techniques can be divided into two categories: parallel techniques using light and serial techniques using matter. The optical lithography techniques have the advantage of being fast because they can expose the entire pattern in parallel. However, these techniques are beginning to reach the limits imposed upon them by the laws of optics, namely, the diffraction limit [3]. The current state of the art in optical lithography that is used in industry can achieve feature sizes on the order of hundreds of nanometers. Efforts are being made to push these limits back by using shorter-wavelength light such as x rays [2], but this presents problems of its own. The serial lithography techniques, such as electron beam lithography [1], can readily attain a resolution on the order of tens of nanometers. However, because of their serial nature these methods are very slow and do not provide a feasible platform for the industrial mass fabrication of nanodevices.

A different avenue for lithography presents itself out of recent developments in the fields of atomic physics and atom optics, namely, the experimental realization of a Bose-Einstein condensate (BEC) [4,5] and the demonstration of the atom interferometer [6–12]. In essence, these developments provide us with the tools needed in order to harness the wave nature of matter. This is advantageous for lithography because the comparatively smaller de Broglie wavelength of atoms readily allows for a lithographic resolution on the nanometer scale. The atom interferometer provides a means of interfering matter waves in order to achieve lithography on such a scale. The BEC, on the other hand, provides a highly coherent and populous source with which to perform this lithography in a parallel fashion. The opportunity thus presents itself to combine the enhanced resolution of matter interferometry with the high throughput of traditional optical lithography.

It should be noted that, although there has been research activity on atom lithography [13–15] for a number of years, most of the work has involved using standing waves of light as optical masks for the controlled deposition of atoms on a substrate. The primary limitations of using such optical masks are that the lithographic pattern cannot be arbitrary and that the resolution of the pattern is limited to the 100 nm scale. Since our scheme uses the atom interferometer, however, it allows for pattern formation by self-interference of a matter wave, and is thus unhampered by the inherent limitations of the optical mask technique.

In this paper we seek to demonstrate theoretically the use of the atom interferometer as a platform for nanolithography by proposing a technique that allows for the manipulation of a single-atom wave packet so as to achieve two-dimensional lithography of an arbitrary pattern on the single-nanometer scale. To do this our scheme employs a lens system along one arm of the interferometer that performs Fourier imaging [3] of the wave-packet component that travels along that arm. By investigating such a technique for a single atom wave packet, we hope to establish the viability of using a similar technique for a single BEC wave packet, which would allow for truly high-throughput lithography.

The paper is organized as follows. Section II presents an overview of the proposed technique. Sections III and IV provide a theoretical analysis of the atom interferometer itself and our proposed imaging system, respectively. Section V is devoted to some practical considerations of the setup and its parameter space, and Sec. VI gives the results of numerical simulations. Finally, we touch upon the issue of replacing the single-atom wave packet with the macroscopic wave function of a BEC in Sec. VII. Appendixes A and B show some of the steps in the derivations.

II. PROPOSED INTERFEROMETER

A. Principles of operation

In a $\pi/2$-π-$\pi/2$ atom interferometer (AI), which was first theoretically proposed by Borde [6] and experimentally demonstrated by Kasevich and Chu [7], an atom beam is released from a trap and propagates in free space until it encounters a $\pi/2$ pulse, which acts as a 50-50 beam splitter [16–22]. The split components then further propagate in free space until they encounter a π pulse, which acts as a mirror so that the trajectories of the split beam components now intersect. The beams propagate in free space again until they encounter another $\pi/2$ pulse at their point of intersection, which now acts as a beam mixer. Because of this beam mixing, any

phase shift ϕ introduced between the beams before they are mixed will cause an interference to occur such that the observed intensity of one of the mixed beams at a substrate will be proportional to $1+\cos\phi$, much as in the Mach-Zehnder interferometer [23] from classical optics. For our scheme we propose the same type of interferometer, but with a single atom released from the trap instead of a whole beam.

Now, if we introduce an arbitrary, spatially varying phase shift $\phi(x,y)$ between the two arms of the interferometer before they mix, the intensity of their interference pattern as observed on a substrate will be proportional to $1+\cos\phi(x,y)$. Thus, in our system, we use an appropriate choice of $\phi(x,y)$ in order to form an arbitrary, two-dimensional pattern. This quantum phase engineering (already demonstrated for BECs [24,25]) is achieved by using the ac-Stark effect so that $I(x,y)\propto\phi(x,y)$, where $I(x,y)$ is the intensity of an incident light pulse.

Also, in order to achieve interference patterns on the nanoscale, $\phi(x,y)$ must itself be at nanometer resolution. However, reliable intensity modulation of a light pulse is limited to the submicrometer range due to diffraction effects. One way to address this is by focusing the wave packet after it is exposed to the submicrometer resolution phase shift $\phi(x,y)$, thereby further scaling down $\phi(x,y)$ to nanometer resolution after it is applied to the wave packet. Our scheme achieves this scaling via an atom lens system.

Additionally, just as with a Gaussian laser beam, exposing a single Gaussian wave packet to a spatially varying phase shift $\phi(x,y)$ will cause it to scatter. In order for both the phase-shifted and non-phase-shifted components of the wave packet to properly interfere, our lens system is also used to perform Fourier imaging [30] such that, at the substrate, the phase-shifted component of the wave packet is an unscattered Gaussian that is properly aligned with its non-phase-shifted counterpart and has the phase information $\phi(x,y)$ still intact. Indeed, the lens system, which is created using the ac-Stark effect, serves the double purpose of scaling down the phase information $\phi(x,y)$ from submicrometer resolution to single-nanometer resolution and neutralizing the wave-packet scattering caused by the same phase shift $\phi(x,y)$.

B. Schematic

In our overall scheme, represented by Fig. 1, the atoms are treated as Λ systems [26–33] (inset B) and are prepared in the ground state $|1\rangle$. A single-atom trap [34–36] is used to release just one atomic wave packet along the z axis. After traveling a short distance, the wave packet is split by a $\pi/2$ pulse into internal states $|1\rangle$ and $|3\rangle$. The state-$|3\rangle$ component gains additional momentum along the y axis and separates from the state-$|1\rangle$ component after they both travel further along the z axis. Next, a π pulse causes the two components to transition their internal states and thereby reflect their trajectories. The component along the top arm is now in the original ground state $|1\rangle$ and proceeds to be exposed to the lens system. The lenses of the lens system are pulses of light that intercept the state-$|1\rangle$ component of the wave packet at different times. By modulating their spatial intensity in the x-y plane, these pulses of light are tailored to impart a particular phase pattern in the x-y plane to the wave-packet component that they interact with via the ac-Stark effect. As shown in inset B, Fig. 1, the detuning of the light that the lenses are composed of is several times larger for state $|3\rangle$ than for state $|1\rangle$. The lenses can therefore be considered to have a negligible ac-Stark effect on the state-$|3\rangle$ wave-packet component as compared to the state-$|1\rangle$ component. This is important, because in a practical situation the separation between the wave packets for $|1\rangle$ and $|3\rangle$ may be small enough so that the transverse extent of the lens pulses could overlap both wave packets.

The first light pulse is intensity modulated to carry the phase information of the first lens of the lens system. It then intercepts the state-$|1\rangle$ wave-packet component and adds the phase $\phi_1(x,y)$. After some time the state-$|1\rangle$ component has evolved due to the first lens such that it is an appropriate size for exposure to the phase information corresponding to the arbitrary pattern image (inset A). Another light pulse is intensity modulated to carry the phase information of both the second lens and the inverse cosine of the arbitrary pattern. The pulse intercepts the state-$|1\rangle$ component and adds the additional phase $\phi_2(x,y)$. After some time a third light pulse is prepared and applied to the state-$|1\rangle$ component to add a phase of $\phi_3(x,y)$, which act as the third lens of the lens system. Soon after, the final $\pi/2$ pulse mixes the trajectories of the wave-packet components. A chemically treated wafer is set to intercept the state-$|1\rangle$ component in the x-y plane. Due to the mixing caused by the last $\pi/2$ pulse, only a part of what is now the state-$|1\rangle$ component has gone through the lens system. Because of the lens system, it arrives at the wafer with a phase that is a scaled-down version of the image phase $\phi_P(x,y)=\arccos P(x,y)$. The other part of what is now the state-$|1\rangle$ component did not go through the lens system. There is therefore a phase difference of $\phi_P(x,y)$ between the two parts of the state-$|1\rangle$ component and the wave packet strikes the wafer in an interference pattern proportional to $1+\cos[\arccos P(x,y)]=1+P(x,y)$. The impact with the wafer alters the chemically treated surface, and the pattern is developed through chemical etching.

As a note, one preparation for the wafer is to coat it with a self-assembled monolayer [37]. However, Hill *et al.* [38] demonstrate an alternate approach using hydrogen passivation, which may be better suited for lithography at the single-nanometer scale due to its inherent atomic-scale granularity.

Finally, note that the coated wafer may reflect as well as scatter the pulses of the lens system. The phase fronts of the wave packets may potentially be distorted if exposed to these reflections and scatterings. However, this problem can be overcome easily as follows. During the time window over which the lens pulses are applied, a small mirror is placed at an angle in front of the wafer, so as to deflect the lens pulses in a harmless direction. This will also have the added benefit of not exposing the wafer to the lens pulses at all. Right after the last lens pulse has been applied and deflected, the mirror will be moved out of the way, thus allowing the atomic waves to hit the wafer surface.

III. ANALYSIS OF THE INTERFEROMETER ($\pi/2$-π-$\pi/2$)

A. Formalism

As explained in the previous section, we consider the behavior of a single-atomic wave packet in our formulation of

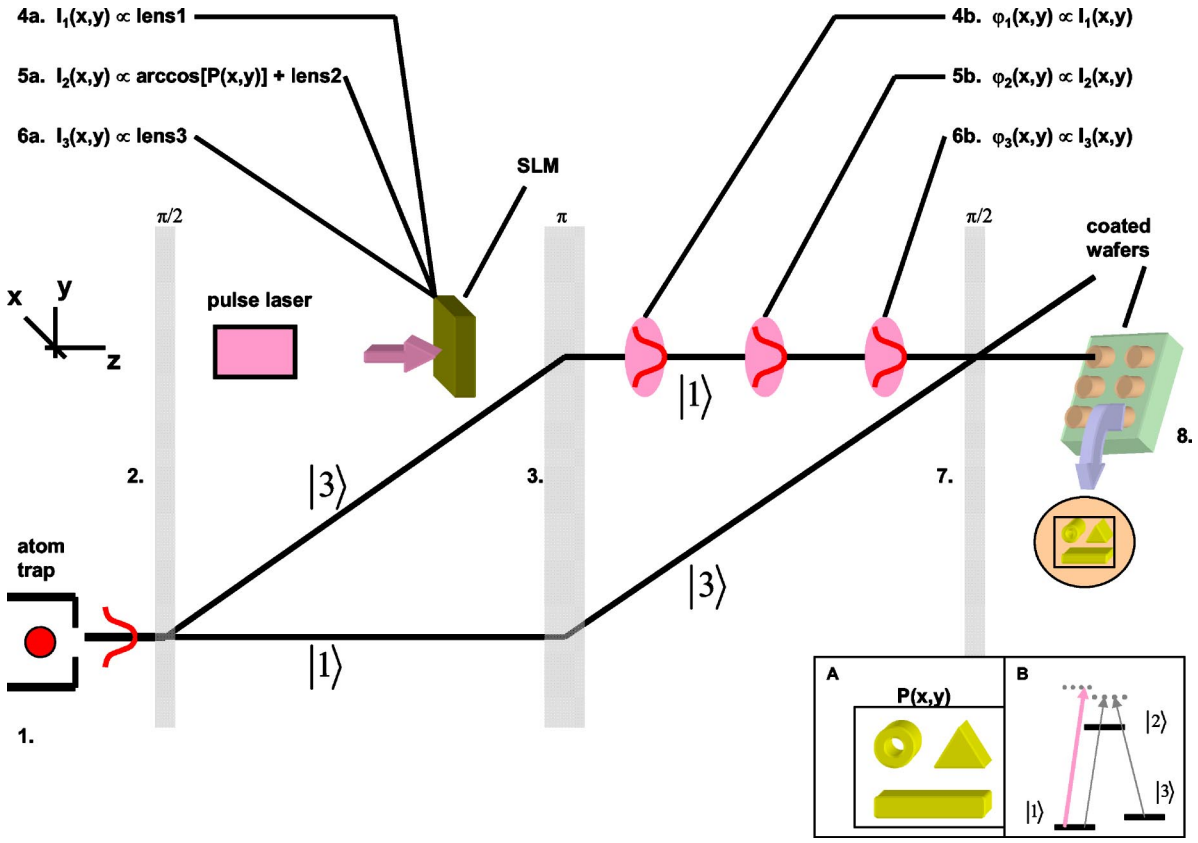

FIG. 1. A single-atomic wave packet is released from the atom trap. (2) The wave packet is split using a $\pi/2$ pulse. (3) The split components are reflected by a π pulse. (4a) The spatial light modulator (SLM) modulates a light pulse such that it will act as the first lens of the atom lens system. (4b) The light pulse intercepts the wave-packet component that is in state $|1\rangle$ and imparts a phase signature $\phi_1(x,y)$ via the ac-Stark effect. (5a) Now the SLM modulates a second light pulse such that it will impart both the phase information corresponding to the arbitrary image $\{\arccos[P(x,y)]\}$ and the phase information of the second lens of the lens system. (5b) The second light pulse intercepts the same wave-packet component as the first one and imparts the phase signature $\phi_2(x,y)$. (6a) The SLM modulates a third light pulse, preparing it to act as the third lens of the lens system. (6b) The third light pulse intercepts the same wave-packet component as the other two pulses and imparts a phase $\phi_3(x,y)$. (7) Both wave-packet components are mixed along the two trajectories by a $\pi/2$ pulse. (8) A chemically treated wafer intercepts the state-$|1\rangle$ component so that an interference pattern forms on the wafer proportional to $1+\cos\{\arccos[P(x,y)]\}=1+P(x,y)$. Inset A: The image $P(x,y)$ that is to be transferred ultimately to the wafer. Inset B: The internal energy states of the wave packet modeled as a Λ system. The light pulses used for the atom lenses have a much larger detuning for ground state $|3\rangle$ than they do for ground state-$|1\rangle$ so that they effectively only interact with the state-$|1\rangle$ component of the wave packet. The $\pi/2$ pulses and the π pulse use light that is largely detuned for both ground states.

the problem. Also, in order to understand and simulate the AI [6–12] properly, the atom must be modeled both internally and externally. It is the internal evolution of the atom while in a laser field that allows for the splitting and redirecting of the beam to occur in the AI. However, the internal evolution is also dependent on the external state. Also, while the external state of the atom accounts for most of the interference effects which result in the arbitrary pattern formation, the internal state is responsible for some nuances here as well.

In following the coordinate system as shown in Fig. 1, we write the initial external wave function as

$$|\Psi_e(\vec{r},t=0)\rangle = \frac{1}{\sigma\sqrt{\pi}}\exp\left(\frac{-|\vec{r}|^2}{2\sigma^2}\right) \tag{1}$$

where $\vec{r}=x\hat{i}+y\hat{j}$.

Internally, the atom is modeled as a three-level Λ system [26–33] (as shown in Fig. 1, inset B) and is assumed to be initially in state $|1\rangle$:

$$|\Psi_i(t)\rangle = c_1(t)|1\rangle + c_2(t)|2\rangle + c_3(t)|3\rangle, \tag{2}$$

where we consider $c_1(0)=1$, $c_2(0)=0$, $c_3(0)=0$. States $|1\rangle$ and $|3\rangle$ are metastable states, while state $|2\rangle$ is an excited state.

As will become evident later, in some cases it is more expedient to express the atom's wave function in k space [39]. To express our wave function, then, in terms of momentum, we first use Fourier theory to reexpress the external wave function as

$$|\Psi_e(x,y,t)\rangle = \frac{1}{2\pi}\int\int |\Phi_e(p_x,p_y,t)\rangle|p_x\rangle|p_y\rangle dp_x dp_y, \quad (3)$$

where we let $|p_x\rangle = e^{i(p_x/\hbar)x}$ and $|p_y\rangle = e^{i(p_y/\hbar)y}$. The complete wave function is simply the outer product of the internal and external states [Eqs. (2) and (3)]:

$$|\Psi(x,y,t)\rangle = \frac{1}{2\pi}\int\int [C_1(p_x,p_y,t)|1,p_x,p_y\rangle + C_2(p_x,p_y,t) \times|2,p_x,p_y\rangle + C_3(p_x,p_y,t)|3,p_x,p_y\rangle]dp_x dp_y, \quad (4)$$

where $C_n(p_x,p_y,t) = c_n(t)|\Phi_e(p_x,p_y,t)\rangle$. In position space, the outer product gives

$$|\Psi(\vec{r},t)\rangle = c_1(t)|1,\Psi_e(\vec{r},t)\rangle + c_2(t)|2,\Psi_e(\vec{r},t)\rangle + c_3(t)|3,\Psi_e(\vec{r},t)\rangle. \quad (5)$$

B. State evolution in free space

The free-space evolution of a wave function is fully derived in Appendix A. Presented here are simply the results cast in our particular formalism. For the free-space Hamiltonian $H = \int\int \Sigma_{n=1}^{3}[(p_x^2+p_y^2)/2m + \hbar\omega_n]|n,p_x,p_y\rangle \times\langle n,p_x,p_y|dp_x dp_y$, if the wave function is known at time $t=0$, then after a duration of time T in free space, the wave function becomes

$$\begin{aligned}|\Psi(\vec{r},t=T)\rangle &= \frac{1}{2\pi}\int\int [C_1(p_x,p_y,0)e^{-i[(p_x^2+p_y^2)/2m\hbar+\omega_1]T}|1,p_x,p_y\rangle \\ &+ C_2(p_x,p_y,0)e^{-i[(p_x^2+p_y^2)/2m\hbar+\omega_2]T}|2,p_x,p_y\rangle \\ &+ C_3(p_x,p_y,0)e^{-i[(p_x^2+p_y^2)/2m\hbar+\omega_3]T}|3,p_x,p_y\rangle]dp_x dp_y, \end{aligned} \quad (6a)$$

or

$$|\Psi(\vec{r},t=T)\rangle = e^{-i\omega_1 T}c_1(0)|1,\Psi_e(\vec{r},T)\rangle + e^{-i\omega_2 T}c_2(0) \times|2,\Psi_e(\vec{r},T)\rangle + e^{-i\omega_3 T}c_3(0)|3,\Psi_e(\vec{r},T)\rangle. \quad (6b)$$

C. State evolution in π and $\pi/2$ pulse laser fields

The electromagnetic fields encountered by the atom at points 2, 3, and 7 in Fig. 1 that act as the $\pi/2$, π, and $\pi/2$ pulses are each formed by two lasers that are counterpropagating in the y-z plane parallel to the y axis. We use the electric dipole approximation to write the Hamiltonian in these fields as

$$\begin{aligned}H = &\int\int \sum_{n=1}^{3}\left(\frac{p_x^2+p_y^2}{2m}+\hbar\omega_n\right)|n,p_x,p_y\rangle\langle n,p_x,p_y|dp_x dp_y \\ &- e_0\vec{\varepsilon}\cdot\frac{\vec{E}_{A0}}{2}[e^{i(\omega_A t - k_A\hat{y}+\phi_A)} + e^{-i(\omega_A t - k_A\hat{y}+\phi_A)}] \\ &- e_0\vec{\varepsilon}\cdot\frac{\vec{E}_{B0}}{2}[e^{i(\omega_B t + k_B\hat{y}+\phi_B)} + e^{-i(\omega_B t + k_B\hat{y}+\phi_B)}], \end{aligned} \quad (7)$$

where $\vec{E}_{A0}$ and $\vec{E}_{B0}$ are vectors denoting the magnitude and polarization of the fields traveling in the $+$ and $-y$ directions, respectively, $\vec{\varepsilon}$ is the position vector of the electron, and e_0 is the electron charge. Refer to Appendix B for the complete derivation of the wave function evolution in these fields. Only the results are presented here.

If the atom begins completely in state $|1,\Psi_e(\vec{r},t)\rangle$ then after a time T of evolving in the above described fields, the result is

$$\begin{aligned}|\Psi(\vec{r},t=T)\rangle = &\cos\left(\frac{\Omega}{2}T\right)|1,\Psi_e(\vec{r},0)\rangle \\ &- ie^{i(\omega_B-\omega_A)T+i(\phi_B-\phi_A)}\sin\left(\frac{\Omega}{2}T\right)|3,\Psi_e(\vec{r},0)\rangle e^{-i(k_A+k_B)y}, \end{aligned} \quad (8)$$

where we have used the definitions given in Sec. III A. We see that for a π pulse ($T=\pi/\Omega$), Eq. (8) becomes

$$|\Psi(x,y,t=\pi/\Omega)\rangle = -ie^{i(\omega_B-\omega_A)\pi/\Omega+i(\phi_B-\phi_A)} \times|3,\Psi_e(x,y,0)\rangle e^{-i(k_A+k_B)y}, \quad (9)$$

while for a $\pi/2$ pulse [$T=\pi/(2\Omega)$], Eq. (8) yields

$$\begin{aligned}&|\Psi(x,y,t=\pi/(2\Omega))\rangle \\ &= \frac{1}{\sqrt{2}}|1,\Psi_e(x,y,0)\rangle - ie^{i(\omega_B-\omega_A)\pi/2\Omega+i(\phi_B-\phi_A)} \\ &\times\frac{1}{\sqrt{2}}|3,\Psi_e(x,y,0)\rangle e^{-i(k_A+k_B)y}. \end{aligned} \quad (10)$$

Similarly, if the atom begins completely in state $|3,\Psi_e(\vec{r},t)\rangle$, the wave function after a time T becomes

$$\begin{aligned}|\Psi(x,y,t=T)\rangle = &-ie^{i(\omega_A-\omega_B)T+i(\phi_A-\phi_B)}\sin\left(\frac{\Omega}{2}T\right) \\ &\times|1,\Psi_e(x,y,0)\rangle e^{i(k_A+k_B)y} + \cos\left(\frac{\Omega}{2}T\right) \\ &\times|3,\Psi_e(x,y,0)\rangle, \end{aligned} \quad (11)$$

so that for a π pulse, Eq. (11) gives

$$|\Psi(x,y,t=\pi/\Omega)\rangle = -ie^{i(\omega_A-\omega_B)\pi/\Omega+i(\phi_A-\phi_B)} \times|1,\Psi_e(x,y,0)\rangle e^{i(k_A+k_B)y}, \quad (12)$$

and for a $\pi/2$ pulse, Eq. (11) becomes

$$\begin{aligned}|\Psi(x,y,t=\pi/(2\Omega))\rangle = &-ie^{i(\omega_A-\omega_B)\pi/2\Omega+i(\phi_A-\phi_B)}\frac{1}{\sqrt{2}} \\ &\times|1,\Psi_e(x,y,0)\rangle e^{i(k_A+k_B)y} \\ &+ \frac{1}{\sqrt{2}}|3,\Psi_e(x,y,0)\rangle. \end{aligned} \quad (13)$$

D. State evolution through the whole interferometer

To see the effects of phase explicitly, we make use of the analysis that we have done for the state evolution of the

wave packet. Take our initial wave packet $|\Psi\rangle$ to have initial conditions as discussed in Sec. III A. At time $t=0$ the first $\pi/2$ pulse equally splits $|\Psi\rangle$ into two components $|\Psi_a\rangle$ and $|\Psi_b\rangle$ such that

$$|\Psi_a\rangle = -ie^{i(\omega_B-\omega_A)\pi/2\Omega+i(\phi_{B1}-\phi_{A1})}\frac{1}{\sqrt{2}}|3,\Psi_e(x,y,0)\rangle e^{-i(k_A+k_B)y}, \tag{14a}$$

$$|\Psi_b\rangle = \frac{1}{\sqrt{2}}|1,\Psi_e(x,y,0)\rangle, \tag{14b}$$

where we used Eq. (8). After a time $t=T_0$ of free space [Eq. (6b)] and then a π pulse, Eqs. (8) and (11) yield

$$|\Psi_a\rangle = -e^{i(\omega_A-\omega_B)\pi/2\Omega+i(\phi_{A2}-\phi_{A1}+\phi_{B1}-\phi_{B2})-i\omega_3T_0}\frac{1}{\sqrt{2}} \times|1,\Psi_e(x,y-y_0,T_0)\rangle, \tag{15a}$$

$$|\Psi_b\rangle = -ie^{i(\omega_B-\omega_A)\pi/\Omega+i(\phi_{B2}-\phi_{A2})-i\omega_1T_0}\frac{1}{\sqrt{2}}|3,\Psi_e(x,y,T_0)\rangle \times e^{-i(k_A+k_B)y}. \tag{15b}$$

The $|\Psi_a\rangle$ component becomes shifted in space by y_0 due to the momentum it gained in the $+y$ direction from the π pulse. Now another zone of free space for a time T_0 [Eq. (7)] followed by the final $\pi/2$ pulse [using Eqs. (8) and (11)] forms

$$\begin{aligned}|\Psi_a\rangle = &-e^{i(\omega_A-\omega_B)\pi/2\Omega+i(\phi_{A2}-\phi_{A1}+\phi_{B1}-\phi_{B2})-i(\omega_1+\omega_3)T_0}\\ &\times\frac{1}{2}|1,\Psi_e(x,y-y_0,2T_0)\rangle\\ &+ie^{i(\phi_{A2}-\phi_{A1}-\phi_{A3}+\phi_{B1}-\phi_{B2}+\phi_{B3})-i(\omega_1+\omega_3)T_0}\\ &\times\frac{1}{2}|3,\Psi_e(x,y-y_0,2T_0)\rangle e^{-i(k_A+k_B)y},\end{aligned} \tag{16a}$$

$$\begin{aligned}|\Psi_b\rangle = &-e^{i(\omega_B-\omega_A)\pi/2\Omega+i(\phi_{B2}-\phi_{B3}-\phi_{A2}+\phi_{A3})-i(\omega_1+\omega_3)T_0}\\ &\times\frac{1}{2}|1,\Psi_e(x,y-y_0,2T_0)\rangle\\ &-ie^{i(\omega_B-\omega_A)\pi/\Omega+i(\phi_{B2}-\phi_{A2})-i(\omega_1+\omega_3)T_0}\\ &\times\frac{1}{2}|3,\Psi_e(x,y-y_0,2T_0)\rangle e^{-i(k_A+k_B)y}.\end{aligned} \tag{16b}$$

Now the $|\Psi_b\rangle$ component is spatially aligned with the $|\Psi_a\rangle$ component. However, another split occurs because both of these components are partially in internal state $|3\rangle$. After some further time T_1 in free space, state $|3\rangle$ has drifted further in the $+y$ direction. The substrate can now intercept the two internal states of the total wave function in separate locations. We write the state-$|1\rangle$ and -$|3\rangle$ wave functions as

$$\begin{aligned}|\Psi_1\rangle = &-\frac{1}{2}(e^{i(\omega_B-\omega_A)\pi/2\Omega+i(\phi_{B2}-\phi_{B3}-\phi_{A2}+\phi_{A3})}\\ &+e^{i(\omega_A-\omega_B)\pi/2\Omega+i(\phi_{A2}-\phi_{A1}+\phi_{B1}-\phi_{B2})})\\ &\times|1,\Psi_e(x,y-y_0,2T_0+T_1)\rangle e^{-i(\omega_1+\omega_3)T_0},\end{aligned} \tag{17a}$$

$$\begin{aligned}|\Psi_3\rangle = &\,i\frac{1}{2}(e^{i(\phi_{A2}-\phi_{A1}-\phi_{A3}+\phi_{B1}-\phi_{B2}+\phi_{B3})}-e^{i(\omega_B-\omega_A)\pi/\Omega+i(\phi_{B2}-\phi_{A2})})\\ &\times|3,\Psi_e(x,y-y_0-y_1,2T_0+T_1)\rangle e^{-i(k_A+k_B)y-i(\omega_1+\omega_3)T_0}.\end{aligned} \tag{17b}$$

These have populations

$$\langle\Psi_1|\Psi_1\rangle = \frac{1}{2}[1+\cos(\phi_0)], \quad \langle\Psi_3|\Psi_3\rangle = \frac{1}{2}[1-\cos(\phi_0)], \tag{18}$$

where $\phi_0=(\pi/\Omega)(\omega_A-\omega_B)-\phi_{A1}+\phi_{B1}+2\phi_{A2}-2\phi_{B2}-\phi_{A3}+\phi_{B3}$. We see that the state populations are functions of the phase differences of the laser fields. Since we can choose these phase differences arbitrarily, we can populate the states arbitrarily. If we choose the phases, for example, such that ϕ_0 is some multiple of 2π, then the wave-packet population will end up entirely in internal state $|1\rangle$.

IV. ARBITRARY IMAGE FORMATION

If, however, between the π pulse and the second $\pi/2$ pulse we apply a spatially varying phase shift $\phi_P(\vec{r})$ to $|\Psi_a\rangle$, but keep ϕ_0 as a multiple of 2π, then the populations in Eqs. (20) become instead

$$\langle\Psi_1|\Psi_1\rangle = \frac{1}{2}\{1+\cos[\phi_P(\vec{r})]\},$$

$$\langle\Psi_3|\Psi_3\rangle = \frac{1}{2}\{1-\cos[\phi_P(\vec{r})]\}. \tag{19}$$

Therefore, if we let $\phi_P(\vec{r})=\arccos[P(\vec{r})]$, where $P(\vec{r})$ is an arbitrary pattern normalized to 1, the state $|1\rangle$ population will be

$$\langle\Psi_1|\Psi_1\rangle = \frac{1}{2}[1+P(\vec{r})]. \tag{20}$$

If the substrate at 8 in Fig. 1 intercepts just this state, the population distribution will be in the form of the arbitrary image. Over time, depositions on the substrate will follow the population distribution, and thereby physically form the image on the substrate.

A. Imparting an arbitrary, spatially varying phase shift for arbitrary image formation

We now review how to do such phase imprinting [24,25] to a single wave packet using the ac-Stark effect. First, consider the Schrödinger equation (SE) for the wave packet expressed in position space:

$$i\hbar\frac{\partial|\Psi(\vec{r},t)\rangle}{\partial t}=\frac{-\hbar^2}{2m}\nabla^2|\Psi(\vec{r},t)\rangle+V(\vec{r})|\Psi(\vec{r},t)\rangle. \quad (21)$$

If we consider a very short interaction time τ with the potential $V(\vec{r})$, we find

$$i\hbar\frac{\partial|\Psi(\vec{r},t+\tau)\rangle}{\partial t}\approx V(\vec{r})|\Psi(\vec{r},t+\tau)\rangle \quad (22a)$$

$$\Rightarrow|\Psi(\vec{r},t+\tau)\rangle\approx|\Psi(\vec{r},t)\rangle e^{-(i/\hbar)V(\vec{r})\tau}. \quad (22b)$$

Thus, we see that an arbitrary phase shift $\phi_P(\vec{r})$ is imparted on the wave packet in position space by choosing $V(\vec{r})=(\hbar/\tau)\phi_P(\vec{r})$. Although this would give the negative of the desired phase, it makes no difference because it is the cosine of the phase that gives the interference pattern.

In order to create the arbitrary potential needed to impart the arbitrary phase shift, we use the ac-Stark effect (light shift). As illustrated in Fig. 1 at 4b, 5b, and 6b, the atom will be in the internal state $|1\rangle$. If exposed to a detuned laser field that only excites the $|1\rangle\rightarrow|2\rangle$ transition, the eigenstates become perturbed such that their energies shift in proportion to the intensity of the laser field. A spatially varying intensity will yield a spatially varying potential energy. Specifically, in the limit that $g/\delta\rightarrow 0$, where g is proportional to the square root of the laser intensity and δ is the detuning, it is found that the energy of the ground state is approximately $\hbar g^2/(4\delta)$. To impart the pattern phase, then, we subject the atomic wave packet at 4b, 5b, and 6b in Fig. 1 to a laser field that has an intensity variation in the x-y plane such that

$$g^2(\vec{r})=(4\delta/\tau)\phi_P(\vec{r})=(4\delta/\tau)\arccos[P(\vec{r})], \quad (23)$$

where $P(\vec{r})$ is the arbitrary pattern normalized to 1 and τ is the interaction time.

B. The need for a lens system

The need for a lens system for the atomic wave packet arises due to two separate considerations. First, there is a need for expanding and focusing the wave packet in order to shrink down the phase pattern imparted at 5b in Fig. 1. We have shown above how the phase pattern is imparted using an intensity variation on an impinging light pulse. However, due to the diffraction limit of light, the scale limit of this variation will be on the order of 100 nm. This will cause the interference at 8 to occur on that scale. To reach a smaller scale, we require a lens system that allows expansion and focusing of the wave packet to occur in the transverse plane. Using such a system, we could, for example, expand the wave packet by two orders of magnitude prior to 5b, impart the phase pattern at 5b, and then focus it back to its original size by the time it reaches 8. The interference would then occur on the scale of 1 nm.

The second consideration that must be made is that an arbitrary phase shift $\phi(x,y)$ introduced at 5b, if it has any variation at all in the transverse plane, will cause the wave packet traveling along that arm of the AI to alter its momentum state. Any free-space evolution after this point will make the wave packet distort or go off trajectrory, causing a noisy interference or even eliminating interference at 8 all together.

Our lens system, then, must accomplish two objectives simultaneously: (1) allow for an expansion and focusing of the wave packet to occur and (2) have the wave packet properly aligned and undistorted when it reaches 8. To do this, we employ techniques similar to those developed in classical Fourier optics [3]. First we develop a diffraction theory for the two-dimensional (2D) quantum-mechanical wave packet; then we use the theory to set up a lens system that performs spatial Fourier transforms on the wave packet in order to achieve the two above stated objectives.

C. Development of the quantum-mechanical wave-function diffraction theory

Consider the 2D SE in freespace

$$i\hbar\frac{\partial|\Psi(\vec{r},t)\rangle}{\partial t}=\frac{-\hbar^2}{2m}\left(\frac{\partial^2}{\partial x^2}+\frac{\partial^2}{\partial y^2}\right)|\Psi(\vec{r},t)\rangle. \quad (24)$$

By inspection, we see that it is linear and shift independent. If we can then find the impulse response of this "system" and convolve it with an arbitrary input, we can get an exact analytical expression for the output. To proceed, we first try to find the transfer function of the system.

Using the method of separation of variables, it is readily shown that all solutions of the system (the 2D SE in free space) can be expressed as linear superpositions of the following function:

$$\Psi(\vec{r},t)=Ae^{[i\vec{k}\cdot\vec{r}-(\hbar/2m)|k|^2t]} \quad (25)$$

where A is some constant and $\vec{k}=k_x\hat{i}+k_y\hat{j}$ can take on any values. Now let us take some arbitrary input to our system at time $t=0$ and express it in terms of its Fourier components:

$$|\Psi_{\text{in}}(\vec{r})\rangle=\frac{1}{2\pi}\int|\Phi_{\text{in}}(\vec{k})\rangle e^{i\vec{k}\cdot\vec{r}}d\vec{k}. \quad (26)$$

We can then evolve each Fourier component for a time T by using Eq. (25) to get the output

$$\begin{aligned}|\Psi_{\text{out}}(\vec{r})\rangle&=\frac{1}{2\pi}\int|\Phi_{\text{in}}(\vec{k})\rangle e^{i[\vec{k}\cdot\vec{r}-(\hbar/2m)|\vec{k}|^2T]}d\vec{k}\\&=\frac{1}{2\pi}\int(|\Phi_{\text{in}}(\vec{k})\rangle e^{-i(\hbar/2m)|\vec{k}|^2T})e^{i\vec{k}\cdot\vec{r}}d\vec{k}\\&=\frac{1}{2\pi}\int|\Phi_{\text{out}}(\vec{k})\rangle e^{i\vec{k}\cdot\vec{r}}d\vec{k}. \quad (27)\end{aligned}$$

It follows that

$$|\Phi_{\text{out}}(\vec{k})\rangle=|\Phi_{\text{in}}(\vec{k})\rangle e^{-i(\hbar/2m)|\vec{k}|^2T}. \quad (28)$$

Our transfer function, then, for a free-space system of time duration T is

$$H(\vec{k})=e^{-i(\hbar/2m)|\vec{k}|^2T}. \quad (29)$$

After taking the inverse Fourier transform, we find the impulse response to be

$$h(\vec{r})=-i\left(\frac{m}{\hbar T}\right)e^{i(m/2\hbar T)|\vec{r}|^2}. \quad (30)$$

Finally, convolving this with some input to the system at time $t=0$, $|\Psi_{\text{in}}(\vec{r})\rangle$, gives the output at time $t=T$, $|\Psi_{\text{out}}(\vec{r})\rangle$, to be

$$|\Psi_{\text{out}}(\vec{r})\rangle = -i\left(\frac{1}{2\pi}\frac{m}{\hbar T}\right)e^{i(m/2\hbar T)|\vec{r}|^2}\int |\Psi_{\text{in}}(\vec{r}')\rangle \times e^{i(m/2\hbar T)|\vec{r}'|^2}e^{-i(m/\hbar T)\vec{r}\cdot\vec{r}'}d\vec{r}'. \quad (31)$$

This expression is analogous to the *Fresnel diffraction integral* from classical optics.

D. Fourier transform lens scheme

Consider now the following.

(1) Take as input some wave function $|\Psi(\vec{r})\rangle$, and use the light shift to apply a "lens" (in much the same way as we show above how to apply the arbitrary pattern phase) such that it becomes

$$|\Psi(\vec{r})\rangle e^{-i(m/2\hbar T)|\vec{r}|^2}.$$

(2) Pass it through the free-space system for a time T using the above derived integral to get

$$-i\left(\frac{1}{2\pi}\frac{m}{\hbar T}\right)e^{i(m/2\hbar T)|\vec{r}|^2}\int |\Psi(\vec{r}')\rangle e^{-i(m/\hbar T)\vec{r}\cdot\vec{r}'}d\vec{r}'$$

(3) Now use the light shift again to create another "lens" where the phase shift is $e^{-i[(m/2\hbar T)|\vec{r}|^2-\pi/2]}$ so that we are left with

$$\left(\frac{1}{2\pi}\frac{m}{\hbar T}\right)\int |\Psi(\vec{r}')\rangle e^{-i(m/\hbar T)\vec{r}\cdot\vec{r}'}d\vec{r}'.$$

We see that this is simply a scaled version of the Fourier transform (FT) of the input. This lens system, then, is such that

$$|\Psi_{\text{out}}(\vec{r})\rangle = \left(\frac{1}{2\pi}\frac{m}{\hbar T}\right)\left|\Phi_{\text{in}}\left(\frac{m}{\hbar T}\vec{r}\right)\right\rangle, \quad (32)$$

where $|\Phi_{\text{in}}\rangle$ is the FT of $|\Psi_{\text{in}}\rangle$.

E. Using the FT lens scheme to create a distortion-free expansion and focusing system for applying the pattern phase

In order to achieve our desired goals of doing expansion and focusing and preventing distortion, we propose the system illustrated in Fig. 2(a). We first input our Gaussian wave packet into a FT scheme with a characteristic time parameter $T=T_A$. We will then get the Fourier transform of the input (also a Gaussian) scaled by $m/(\hbar T_A)$. Then, we give the wave packet a phase shift that corresponds to the desired interference pattern (pattern phase) and put it through another FT scheme with the same time parameter T_A. The wave function is now the convolution of the original input with the pattern phase. Finally, a third FT scheme is used with $T=T_B$ so that the output is the same as the wave function just before the second FT scheme, but is now reflected about the origin and scaled by $m/(\hbar T_B)$ instead of $m/(\hbar T_A)$. The pattern phase, therefore, has been scaled down by a factor of T_A/T_B. Since both T_A and T_B can be chosen arbitrarily, we can, in principle, scale down the pattern phase by orders of magnitude. If, for example, the pattern phase is first imparted on a scale of $\sim$100 nm, we can choose T_A/T_B to be 100 so that at the output of our lens system, it is on a scale of $\sim$1 nm. By scaling down the pattern phase, we can scale down the interference pattern at point 8 in Fig. 1.

Within the context of the interferometer, our lens system is placed at 4b, 5b, and 7 in Fig. 1. Now, since the system provides us with the desired output immediately in time after the final lens [lens 3b in Fig. 2(a)], this final lens, the final $\pi/2$ pulse, and the substrate 6 all need to be adjacent. If they are not, the wave packet will undergo extra free-space evolution and may distort. However, such a geometry is difficult to achieve experimentally so we propose a modification to the lens system [Fig. 2(b)]. Specifically, we can move the lens 3b in Fig. 2(a) to occur immediately before lens 2a, as long as we rescale it to account for the different wave-packet size at that location. We call the rescaled version 3b′, which is the same as 3b except for the parameter T_A in place of T_B. We can then place the substrate at 8 in Fig. 2(a) to be where the lens 3b previously was; that is, a time T_B away from lens 3a. The final $\pi/2$ pulse can occur anywhere between lens 3a and the substrate, as long as it is far enough away from the substrate to allow sufficient time for the state-$|3\rangle$ component to separate from the state-$|1\rangle$ component. To avoid disturbing the requisite symmetry of the AI, we accomplish this by choosing T_B to be sufficiently large while leaving the final $\pi/2$ pulse itself in its original location. This geometry will allow the substrate to intercept the state-$|1\rangle$ component exclusively and at precisely the right moment such that it does not undergo too little or too much free-space evolution without having any of the final $\pi/2$ pulse, final lens, or substrate adjacent. Finally, we can simplify the lens system's implementation if we combine the lenses that are adjacent. Lenses 1b, 2a, 3b′, and $\phi_P(\vec{r})$ can be combined into lens α; lenses 2b and 3a can be combined into lens β. Explicitly, lens α has phase shift

$$\phi_\alpha(\vec{r}) = -\left(\frac{3m}{2\hbar T_A}\right)|\vec{r}|^2 + \pi - \phi_P(\vec{r}) \quad (33)$$

and lens β has phase shift

$$\phi_\beta(\vec{r}) = -\left(\frac{m}{2\hbar T_A}+\frac{m}{2\hbar T_B}\right)|\vec{r}|^2 + \frac{\pi}{2}. \quad (34)$$

Figure 2(c) shows the implementation of the lens system within the context of the whole AI.

A cause for concern may arise in the fact that with the lens system in place, the part of the wave packet that travels along the arm without the lens will be interfering not with a phase-modified version of itself, but with a phase-modified Fourier transform of itself. That is, the output of the lens system is a phase-modified Fourier transform of its input. As such, the effective width of the wave packet coming from the lens system may be significantly larger than the effective width of that coming from the arm without lenses, thus causing a truncation of the pattern formation around the edges. This problem is addressed by selecting T_B such that the wave

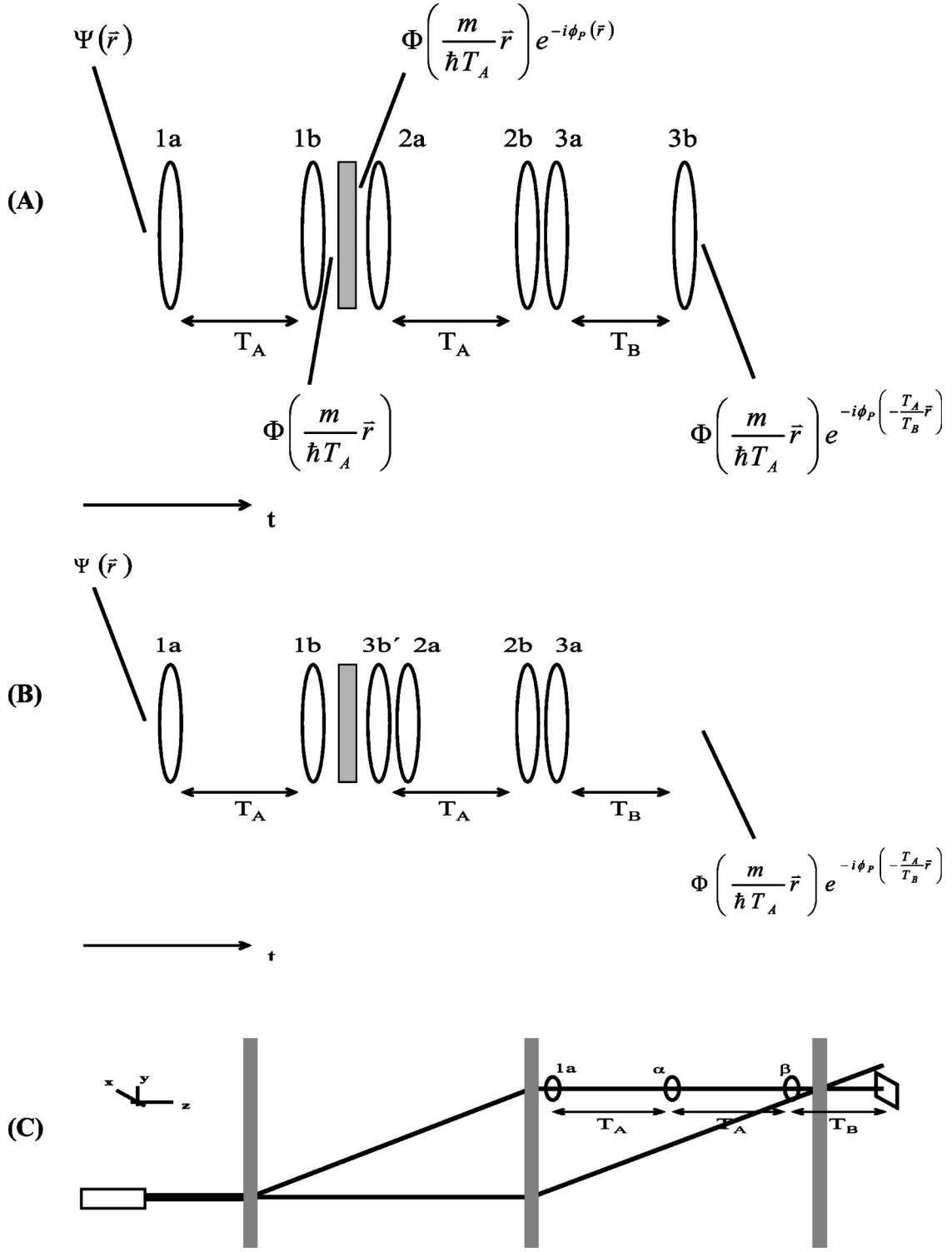

FIG. 2. (A) The lens system. Each lens is actually a pulse of light with a transverse intensity modulation. Between lenses 1a and 1b and 2a and 2b are free-space regions of time duration T_A, while between lenses 3a and 3b there is a free-space region of duration T_B. Lenses 1a and 2a give the wave function a phase $\phi_{1a}=\phi_{2a}=-(m/2\hbar T_A)|\vec{r}|^2$, lenses 1b and 2b impart a phase $\phi_{1b}=\phi_{2b}=-(m/2\hbar T_A)|\vec{r}|^2+\pi/2$, lens 3a gives a phase $\phi_{3a}=-(m/2\hbar T_B)|\vec{r}|^2$, and lens 3b gives a phase $\phi_{3b}=-(m/2\hbar T_B)|\vec{r}|^2+\pi/2$. (B) The lens system from (A) rearranged. The input and output are still the same, but the output is no longer immediately preceded by a lens. Lens 3b is the same as lens 3b from (A) except for T_A in place of T_B so that it gives a phase shift of $\phi_{3b'}=-(m/2\hbar T_A)|\vec{r}|^2+\pi/2$. (C) The modified lens system in context. Lenses α and β are composites of the lenses from the system of (B). Between lenses 1a and α is a free-space region of time length T_A, as well as between lenses α and β. Between lens β and the substrate is a free-space region of time duration T_B. Values of $\phi_\alpha(\vec{r})$ and $\phi_\beta(\vec{r})$ are as in Eqs. (33) and (34), respectively.

packet from the lens system is scaled to have an effective width equivalent to or smaller than the wave packet from the other arm. Also, because of the Fourier transform, the wave packet coming from the lens system, even without an added pattern phase, may have a different phase signature from the wave packet coming from the other arm. Regarding this issue, our numerical experiments show that after free-space propagation for a time on the order of the time scale determined as practical (see Sec. V), the phase difference between the original wave packet and its Fourier transform is very small over the span of the effective width of the wave packet. Thus, the effect of this phase noise on the interference pattern is negligible.

V. SOME PRACTICAL CONSIDERATIONS

A. Wave-packet behavior

The behavior of the wave packet primarily has implications for the time and wave-packet effective width parameters of the lithography scheme. As mentioned earlier, the scale limit of the intensity variation that creates the pattern phase when it is first applied is $\sim 10^{-7}$ m. The lens system then further reduces the scale of the pattern phase by a factor of T_A/T_B. To achieve lithography features on the scale of ~ 1 nm, this ratio needs to be ~ 100. However, we must also take into consideration the extent of the entire intensity variation. In other words, referring to Fig. 2(c), the effective width of the wave packet at lens α must be large enough to accommodate the entire pattern on the light pulse bearing the phase pattern information. We assume that this dimension will be on the order of a millimeter. We know that the wave packet at lens α is a scaled Fourier transform of the wave packet immediately before lens 1a, so that its effective width at lens α is $\hbar T_A/m\sigma_{\text{in}}$. This must be on the order of 10^{-3} m. Also, another way in which the time parameters are restricted is by the total amount of time that the atom spends in the AI.

Now, as shown earlier, it is the state-$|1\rangle$ component in our scheme that will form the desired interference pattern. The substrate must therefore intercept this component exclusive of the state-$|3\rangle$ component. Fortunately, the state-$|3\rangle$ component will have an additional velocity in the y direction due to photon recoil so that the two states will separate if given enough time. Also recall that each wave-packet state after the final $\pi/2$ pulse is composed of two elements, one that went through the lens system and one that did not, such that the elements that traveled along the arm without the lens system will have larger effective widths (since the output of the lens system is smaller than its input). The two states will be sufficiently separated, then, when the state-$|3\rangle$ component has traveled far enough in the $+y$ direction after the final $\pi/2$ pulse such that there is no overlap of the larger effective widths. Since we know that photon recoil gives the state-$|3\rangle$ component an additional momentum of $2\hbar k$ in the $+y$ direction, we have $mv=2\hbar k$. Also, it can be shown that the effective width of a wave packet after passing through free space for a time T is $\sigma\sqrt{1+(T/\tau)}$, where $\tau=m\sigma/\hbar$ and σ is the original effective width. Therefore, for sufficient spatial separation of the states (assuming that the time between the final $\pi/2$ pulse and the substrate is on the order of T_B) we need $v\times T_B \gtrsim \sigma_{\text{in}}\sqrt{1+(T_B/\tau)}$.

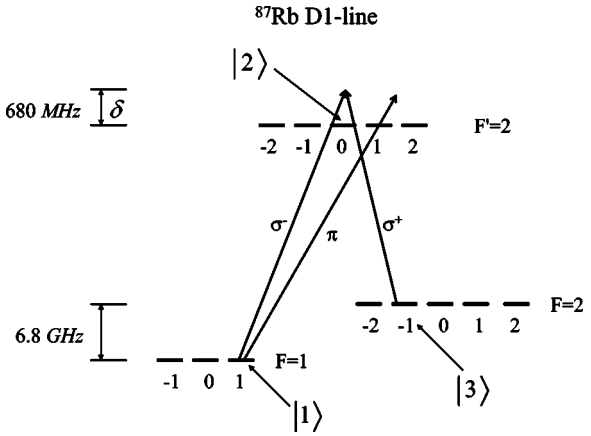

FIG. 3. The poposed transition scheme. We consider $5^2S_{1/2}(F=1,m=1)\equiv|1\rangle$, $5^2P_{1/2}(F'=2,m=0)\equiv|2\rangle$, and $5^2S_{1/2}(F=2,m=-1)\equiv|1\rangle$, where the quantization axis corresponds to the $\hat{y}$ direction in Fig. 1. σ^--polarized light excites the $|1\rangle\leftrightarrow|2\rangle$ transition and σ^+-polarized light excites the $|2\rangle\leftrightarrow|3\rangle$ transition. Both lasers are detuned by 680 MHz. For the $\pi/2$, π, and $\pi/2$ pulses, the above mentioned two transitions are simultaneously excited. For the light-shift-based lens system, as shown in the picture, a different transition from the state $|1\rangle$ to the sublevel $5^2P_{1/2}(F'=2,m=1)$ is used, and π-polarized light is applied. Since this field is highly detuned from the $F=2\leftrightarrow F'=2$ transitions, the light shift for $|3\rangle$ can be neglected.

To summarize, our restrictions are

$$T_A \lesssim 10 \text{ s}, \quad T_B \lesssim 10^{-2}T_A,$$

and

$$\frac{\hbar T_A}{m\sigma_{\text{in}}} \gtrsim 10^{-3} \text{ m}, \quad \frac{2\hbar}{m}T_B \gtrsim \sigma_{\text{in}}\sqrt{1+\left(\frac{\hbar T_B}{m\sigma_{\text{in}}}\right)}.$$

After using some simple algebra, we find that the first three restrictions are satisfied if we apply the following

$$\sigma_{\text{in}} \lesssim 10^{-5} \text{ m}, \quad \sim \sigma_{\text{in}}/T_A \lesssim 10^{-6} \text{ m/s } T_B \lesssim 10^{-2}T_A.$$

We can, for example, choose $\sigma_{\text{in}}=10^{-5}$ m, $T_A\sim 10$ s, $T_B \sim 10^{-1}$ s. A simple check shows that these choices also satisfy the fourth restriction.

Finally, since our proposed lithography scheme involves the use of a single atom at a time, it entails the drawback of being very slow. To make this type of lithography truly practical, a Bose-Einstein condensate [4,5] would have to be used instead of a single-atomic wave packet.

B. Proposed ^{87}Ru levels and transitions for the nanolithography scheme

For practical implementation of our three-level atom, we use the $D1$ transitions in ^{87}Rb [40]. Figure 3 illustrates. One of the restrictions is that, in order to be able to neglect spontaneous emission, we need for each single transition

$$\left(\frac{g_0}{\delta}\right)^2 \times \Gamma \times \tau \ll 1, \tag{35}$$

where g_0 is the Rabi frequency, δ is the detuning, Γ is the decay rate, and τ is the interaction time. Both the Raman pulse scheme and the light shift scheme also require

$$g_0 \ll \delta. \tag{36}$$

We have the following relation:

$$g_{0,\max}^2 = \left(\frac{I_{\max}}{I_{\text{sat}}}\right)\Gamma^2. \tag{37}$$

If we assume $I_{\text{sat}}=3\ \text{mW/cm}^2$, $I_{\max}=2\ \text{mW/mm}^2$, and $\Gamma=3.33\times10^7\ \text{s}^{-1}$, we find that $g_{0,\max}\approx 8.6\times10^9$ Hz.

We choose the relevant Raman Λ transition levels to be $|1\rangle \equiv 5\,^2S_{1/2}(F=1,m=1)$, $|2\rangle \equiv 5\,^2P_{1/2}(F=2,m=0)$, and $5\,^2S_{1/2}(F=2,m=-1)\equiv|3\rangle$, with the quantization axis being in the $\hat{y}$ direction of Fig. 1. The energy difference between the levels $|1\rangle$ and $|2\rangle$ is 6.8 GHz. The $|1\rangle\rightarrow|2\rangle$ and $|2\rangle\rightarrow|3\rangle$ transitions are performed by simultaneously applying σ^-- and σ^+-polarized fields. The two ground states $|1\rangle$ and $|3\rangle$ have equal and opposite g factors, so that they will experience the same force for a given magnetic field gradient used for slowing them. For the ac-Stark shift, we apply π-polarized light that couples $|1\rangle$ to the $F'=2,m=1$ excited state. Because this field is highly detuned from the $F=2\leftrightarrow F'=2$ transition, the corresponding light shift of level $|3\rangle$ can be neglected.

In order to satisfy the constraint that the Rabi frequency be much less than the detuning, we choose $g_0=68$ MHz. This is well below the maximum limit calculated above.

As far as the interaction time for the $\pi/2$ and π pulse scheme, it is the Raman Rabi frequency that is of interest:

$$\Omega = \frac{g_0^2}{2\delta}. \tag{38}$$

Using this in Eq. (36), we get

$$2\frac{\Omega}{\delta} \times \Gamma \times \tau \ll 1$$

$$\Rightarrow \Omega\tau \ll \frac{\delta}{2\Gamma}. \tag{39}$$

Plugging in the chosen value for δ and the typical value of 33.33 MHz for Γ, we find that $\Omega\tau \ll 10.2$. We can satisfy this restraint by choosing $\Omega\tau=\pi$ for the π pulse and half as much for the $\pi/2$ pulse, giving a pulse duration of $\tau=\pi/\Omega \approx 924$ ns for a π pulse and $\tau\approx 462$ ns for a $\pi/2$ pulse.

For the light shift we use the same π-polarized excitation of state $|1\rangle\rightarrow 5\,^2P_{1/2}(F'=2,m=1)$ as shown in Fig. 3. The time constraint in this case is

$$\frac{g_0^2}{4\delta}\tau = 2\pi. \tag{40}$$

This gives an interaction time of $\tau\approx 3.7\ \mu$s. Ideally, the light shift pulse will only interact with the wave packet in state $|1\rangle$. This may actually be possible if we choose T_A to be large enough such that the two states gain enough of a transverse separation. If, as by example above, we choose $T_A \sim 10$ s, then the separation between the two states will be on the order of a centimeter and there will be virtually no overlap between the two components of the wave packet in the separate arms. The light pulse could then simply intercept only state $|3\rangle$. If, however, the situation is such that the states are overlapping, then state $|1\rangle$ will also experience the light shift, but it will be about a factor of ten less because of the detuning being approximately ten times larger for it than for the state-$|3\rangle$ transition.

VI. NUMERICAL EXPERIMENTS

The numerical implementation of our lithography scheme was done by distributing the wave packets across finite meshes and then evolving them according to the Schrödinger equation. This evolution was done in both position and momentum space according to expediency. To go between the two domains, we used two-dimensional Fourier transform and inverse Fourier transform algorithms.

The initial wave packet was taken in momentum space and completely in internal state $|1\rangle$. Specifically, the wave packet was given by the Fourier transform of Eq. (1):

$$|\Phi_e(\vec{k},t=0)\rangle = \sqrt{\frac{\sigma}{\sqrt{\pi}}}\exp\left(\frac{-|\vec{k}|^2\sigma^2}{2}\right). \tag{41}$$

The evolution of the wave packets in the π and $\pi/2$ pulses was done in momentum space in order to be able to account for the different detunings that result for each momentum component due to the Doppler shift. Specifically, we numerically solved Eq. (B15) for the different components of the k-space wave packet mesh, then applied the inverse of the transformation matrix given by Eq. (B9) to go to the original basis.

Outside of the lens system, the free-space evolution of the wave packets was also done in momentum space. This was achieved easily by using Eqs. (A4). Within the lens system, however, it was more computationally efficient to use Eq. (31) for the free-space evolution because of the need to apply the lenses in position space. The results of using Eq. (32) were initially cross-checked with the results of using Eqs. (A4) and were found to agree.

Figure 4(a) is a targeted (arbitrary) pattern. Figures 4(b) and 4(c) demonstrate the formation of the arbitrary pattern by interference of the state-$|1\rangle$ wave packets at the output of the interferometer. Both figures were the result of applying the same arbitrary pattern phase, but Fig. 4(b) was formed without any shrinking implemented (i.e., $T_A=T_B$). Figure 4(c), however, demonstrates the shrinking ability of the lens system by yielding a version of Fig. 4(b) that is scaled by a factor of $2(T_A/T_B=2)$. The length scales are in arbitrary units due to the use of naturalized units for the sake of computational viability.

VII. SUGGESTIONS FOR EXTENSION TO BEC

As mentioned above, in order to make the lithography scheme truly practical, a Bose-Einstein condensate is re-

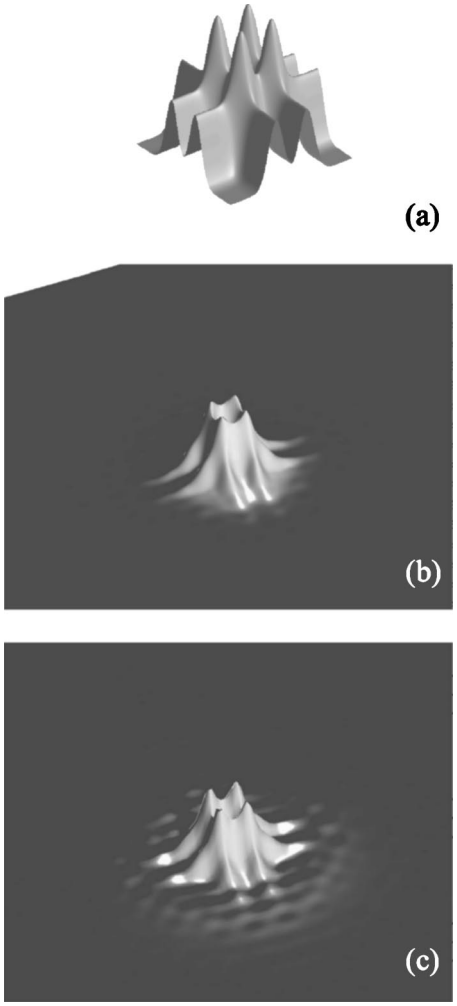

FIG. 4. (a) A targeted arbitrary (e.g., a tic-tac-toe board here) image. (b) The arbitrary image is now formed with the lens system in place, but without any scaling. We see that it is a more complex pattern than just a simple periodic structure such as sinusoidal fringes. (c) The same image as in (b) is formed with the lens system still in place, but a scaling factor of 2 has been used to shrink the pattern.

quired in place of the single atom. Indeed, the self-interference of a BEC has already been demonstrated [41,42]. The difficulty in using the BEC for controlled imaging, however, arises from the nonlinear term in the Gross-Pitaevskii equation (GPE). Our lens system, for example, would not be valid as it was developed from the linear SE.

One approach to getting around this problem is to try to eliminate the nonlinear term in the GPE. Specifically, the GPE for the BEC takes the form

$$i\hbar\frac{\partial\Psi}{\partial t}=\left(\frac{-\hbar^2}{2m}\nabla^2+V+U_0|\Psi|^2\right)\Psi, \tag{42}$$

where the nonlinear term coefficient is $U_0=4\pi\hbar^2a/m$ and a is the scattering length for the atom. It has been demonstrated for ^{87}Rb that the scattering length can be tuned over a broad range by exposing the BEC to magnetic fields of varying strength near Feshbach resonances [43,44]. The relationship between the scattering length and the applied magnetic field B when near a Feshbach resonance can be written as

$$a=a_{\mathrm{bg}}\left(1-\frac{\Delta}{B-B_{\mathrm{peak}}}\right), \tag{43}$$

where a_{bg} is the background scattering length, B_{peak} is the resonance position, and $\Delta=B_{\mathrm{zero}}-B_{\mathrm{peak}}$. Setting $B=B_{\mathrm{zero}}$ would therefore set the scattering length to zero and eliminate the nonlinear term in the GPE. While the atom-atom interaction may not be completely eliminated in reality due to the fluctuation in density that we wish to effect through the lens system, it is worth investigating if it could be made to be negligible over an acceptable range. We could then use our previously developed lens system to perform the imaging and thereby interfere a large number of atoms simultaneously. Alternatively, one must redevelop the design of the lenses and the imaging optics as applied to the equation of motion for a BEC [Eq. (42)] for a nonzero value of U_0. This effort is in progress.

ACKNOWLEDGMENTS

This work was supported by DARPA Grant No. F30602-01-2-0546 under the QUIST program, ARO Grant No. DAAD19-001-0177 under the MURI program, NRO Grant No. NRO-000-00-C-0158, and AFOSR Grants: No. F49620-02-1-0400 and No. FA9550-04-1-0189.

APPENDIX A: STATE EVOLUTION IN FREE SPACE

In free space, the Hamiltonian can be expressed in the momentum domain as

$$H=\int\int\sum_{n=1}^{3}\left(\frac{p_x^2+p_y^2}{2m}+\hbar\omega_n\right)|n,p_x,p_y\rangle\langle n,p_x,p_y|dp_xdp_y, \tag{A1}$$

where ω_n is the frequency corresponding to the eigenenergy of internal state $|n\rangle$. For a single momentum component ($p_x=p_{x0}$ and $p_y=p_{y0}$), the Hamiltonian for the total evolution in momentum space is given by

$$H=\begin{bmatrix}\frac{p_{x0}^2+p_{y0}^2}{2m}+\hbar\omega_1 & 0 & 0\\ 0 & \frac{p_{x0}^2+p_{y0}^2}{2m}+\hbar\omega_2 & 0\\ 0 & 0 & \frac{p_{x0}^2+p_{y0}^2}{2m}+\hbar\omega_3\end{bmatrix}. \tag{A2}$$

Using this in the SE, we get the equations of the amplitude evolution in momentum space:

$$\dot{C}_1(p_{x0},p_{y0},t)=-\frac{i}{\hbar}\left(\frac{p_{x0}^2+p_{y0}^2}{2m}+\hbar\omega_1\right)C_1(p_{x0},p_{y0},t),$$

$$\dot{C}_2(p_{x0},p_{y0},t)=-\frac{i}{\hbar}\left(\frac{p_{x0}^2+p_{y0}^2}{2m}+\hbar\omega_2\right)C_2(p_{x0},p_{y0},t), \tag{A3}$$

$$\dot{C}_3(p_{x0},p_{y0},t) = -\frac{i}{\hbar}\left(\frac{p_{x0}^2+p_{y0}^2}{2m}+\hbar\omega_3\right)C_3(p_{x0},p_{y0},t).$$

These yield the solutions

$$C_1(p_{x0},p_{y0},t) = C_1(p_{x0},p_{y0},0)e^{-i[(p_{x0}^2+p_{y0}^2)/2m\hbar+\omega_1]t},$$

$$C_2(p_{x0},p_{y0},t) = C_2(p_{x0},p_{y0},0)e^{-i[(p_{x0}^2+p_{y0}^2)/2m\hbar+\omega_2]t}, \quad \text{(A4)}$$

$$C_3(p_{x0},p_{y0},t) = C_3(p_{x0},p_{y0},0)e^{-i[(p_{x0}^2+p_{y0}^2)/2m\hbar+\omega_3]t}.$$

We see that if the wave function is known at time $t=0$, then after a duration of time T in free space, the wave function becomes

$$\begin{aligned}|\Psi(\vec{r},t=T)\rangle &= \frac{1}{2\pi}\int\int [C_1(p_x,p_y,0)e^{-i[(p_x^2+p_y^2)/2m\hbar+\omega_1]T}|1,p_x,p_y\rangle \\ &+ C_2(p_x,p_y,0)e^{-i[(p_x^2+p_y^2)/2m\hbar+\omega_2]T}|2,p_x,p_y\rangle \\ &+ C_3(p_x,p_y,0)e^{-i[(p_x^2+p_y^2)/2m\hbar+\omega_3]T}|3,p_x,p_y\rangle]dp_xdp_y. \end{aligned} \quad \text{(A5)}$$

We can also write it as

$$\begin{aligned}|\Psi(\vec{r},t=T)\rangle = e^{-i\omega_1 T}c_1(0)|1,\Psi_e(\vec{r},T)\rangle + e^{-i\omega_2 T}c_2(0) \\ \times|2,\Psi_e(\vec{r},T)\rangle + e^{-i\omega_3 T}c_3(0)|3,\Psi_e(\vec{r},T)\rangle. \end{aligned} \quad \text{(A6)}$$

APPENDIX B: STATE EVOLUTION IN π AND $\pi/2$ PULSE LASER FIELDS

The electromagnetic fields encountered by the atom at points 2, 3, and 7 in Fig. 1 that act as the π and $\pi/2$ pulses are each formed by two lasers that are counterpropagating in the y-z plane parallel to the y axis. We will refer to the laser propagating in the $+y$ direction as $\vec{E}_A$, and the one propagating in the $-y$ direction as $\vec{E}_B$. In deriving the equations of motion under this excitation, we make the following assumptions: (1) the laser fields can be treated semiclassically [45], (2) the intensity profiles of the laser fields forming the π and $\pi/2$ pulses remain constant over the extent of the atomic wave packet, (3) the wavelengths of the lasers are significantly larger than the separation distance between the nucleus and electron of the atom, (4) $\vec{E}_A$ excites only the $|1\rangle\leftrightarrow|2\rangle$ transition and $\vec{E}_B$ only the $|3\rangle\leftrightarrow|2\rangle$ transition, (5) $\vec{E}_A$ and $\vec{E}_B$ are far detuned from the transitions that they excite, and (6) $\vec{E}_A$ and $\vec{E}_B$ are of the same intensity.

Using assumptions (1) and (2), we write the laser fields as

$$\begin{aligned}\vec{E}_A &= \vec{E}_{A0}\cos(\omega_A t - k_A\hat{y} + \phi_A) \\ &= \frac{\vec{E}_{A0}}{2}[e^{i(\omega_A t - k_A\hat{y}+\phi_A)} + e^{-i(\omega_A t - k_A\hat{y}+\phi_A)}] \end{aligned} \quad \text{(B1)}$$

and

$$\begin{aligned}\vec{E}_B &= \vec{E}_{B0}\cos(\omega_B t + k_B\hat{y} + \phi_B) \\ &= \frac{\vec{E}_{B0}}{2}[e^{i(\omega_B t + k_B\hat{y}+\phi_B)} + e^{-i(\omega_B t + k_B\hat{y}+\phi_B)}] \end{aligned} \quad \text{(B2)}$$

where $\vec{E}_{A0}$ and $\vec{E}_{B0}$ are vectors denoting the magnitude and polarization of their respective fields. Keeping in mind that our wave function is expressed in the momentum domain, we take position as an operator.

The Hamiltonian here is expressed as the sum of two parts: $H=H_0+H_1$. The first part corresponds to the noninteraction energy:

$$H_0 = \int\int\sum_{n=1}^{3}\left(\frac{p_x^2+p_y^2}{2m}+\hbar\omega_n\right)|n,p_x,p_y\rangle\langle n,p_x,p_y|dp_xdp_y. \quad \text{(B3)}$$

The second part accounts for the interaction energy, for which we use assumption (3) from above to make the electric dipole approximation and get

$$\begin{aligned}H_1 = &-e_0\vec{\varepsilon}\cdot\frac{\vec{E}_{A0}}{2}[e^{i(\omega_A t - k_A\hat{y}+\phi_A)} + e^{-i(\omega_A t - k_A\hat{y}+\phi_A)}] \\ &- e_0\vec{\varepsilon}\cdot\frac{\vec{E}_{B0}}{2}[e^{i(\omega_B t + k_B\hat{y}+\phi_B)} + e^{-i(\omega_B t + k_B\hat{y}+\phi_B)}] \end{aligned} \quad \text{(B4)}$$

where $\vec{\varepsilon}$ is the position vector of the electron, and e_0 is the electron charge. Now, seeing that expressions of the form $\langle n|\vec{\varepsilon}\cdot\vec{E}_{A0}|n\rangle$ and $\langle n|\vec{\varepsilon}\cdot\vec{E}_{B0}|n\rangle$ are zero, and using assumption (4), we can express Eq. (B4) as

$$\begin{aligned}H_1 = \int\int\Bigg[&\frac{\hbar g_A}{2}(|1,p_x,p_y\rangle\langle 2,p_x,p_y| + |2,p_x,p_y\rangle\langle 1,p_x,p_y|) \\ &\times[e^{i(\omega_A t - k_A\hat{y}+\phi_A)} + e^{-i(\omega_A t - k_A\hat{y}+\phi_A)}] + \frac{\hbar g_B}{2}(|3,p_x,p_y\rangle \\ &\times\langle 2,p_x,p_y| + |2,p_x,p_y\rangle\langle 3,p_x,p_y|)[e^{i(\omega_B t + k_B\hat{y}+\phi_B)} \\ &+ e^{-i(\omega_B t + k_B\hat{y}+\phi_B)}]\Bigg]dp_xdp_y, \end{aligned} \quad \text{(B5)}$$

where we let $g_A=\langle 1|\vec{\varepsilon}\cdot\vec{E}_{A0}|2\rangle=\langle 2|\vec{\varepsilon}\cdot\vec{E}_{A0}|1\rangle$ and $g_B=\langle 3|\vec{\varepsilon}\cdot\vec{E}_{B0}|2\rangle=\langle 2|\vec{\varepsilon}\cdot\vec{E}_{B0}|3\rangle$. Finally, we can use the identities [39]

$$e^{ik\hat{y}} = \sum_n\int\int|n,p_x,p_y\rangle\langle n,p_x,p_y-\hbar k|dp_xdp_y, \quad \text{(B6a)}$$

$$e^{-ik\hat{y}} = \sum_n\int\int|n,p_x,p_y\rangle\langle n,p_x,p_y+\hbar k|dp_xdp_y, \quad \text{(B6b)}$$

and the rotating wave approximation [45] in Eq. (B5) to give

$$H_1 = \int\int \left[\frac{\hbar g_A}{2} e^{i(\omega_A t+\phi_A)} |1,p_x,p_y\rangle\langle 2,p_x,p_y+\hbar k_A| \right.$$
$$+ \frac{\hbar g_A}{2} e^{-i(\omega_A t+\phi_A)} |2,p_x,p_y+\hbar k_A\rangle\langle 1,p_x,p_y| + \frac{\hbar g_B}{2} e^{i(\omega_B t+\phi_B)}$$
$$\times |3,p_x,p_y+\hbar k_A+\hbar k_B\rangle\langle 2,p_x,p_y+\hbar k_A| + \frac{\hbar g_B}{2} e^{-i(\omega_B t+\phi_B)}$$
$$\left. \times |2,p_x,p_y+\hbar k_A\rangle\langle 3,p_x,p_y+\hbar k_B+\hbar k_A| \right] dp_x dp_y. \quad \text{(B7)}$$

We note that the full interaction between the internal states $|1\rangle$, $|2\rangle$, and $|3\rangle$ occurs across groups of three different momentum components: $|p_x,p_y\rangle$, $|p_x,p_y+\hbar k_A\rangle$, and $|p_x,p_y+\hbar k_A+\hbar k_B\rangle$. This can be understood physically in terms of photon absorption and emission and conservation of momentum. Keeping in mind assumption (4), if an atom begins in state $|1,p_{x0},p_{y0}\rangle$ and absorbs a photon from field $\vec{E}_A$, it will transition to internal state $|2\rangle$ because it has become excited, but it will also gain the momentum of the photon ($\hbar k_A$) traveling in the $+y$ direction. It will therefore end up in state $|2,p_{x0},p_{y0}+\hbar k_A\rangle$. Now the atom is able to interact with field $\vec{E}_B$, which can cause stimulated emission of a photon with momentum $\hbar k_B$ in the $-y$ direction. If such a photon is emitted, the atom itself will gain an equal momentum in the opposite direction, bringing it into external state $|p_{x0},p_{y0}+\hbar k_A+\hbar k_B\rangle$. The atom will also make an internal transition to state $|3\rangle$ because of the deexcitation. The total state will now be $|3,p_{x0},p_{y0}+\hbar k_A+\hbar k_B\rangle$. We thereby see that our mathematics is corroborated by physical intuition.

Getting back to the Hamiltonian, we look at the general case of one momentum grouping so that we get in matrix form $H=H_0+H_1$ from Eqs. (B3) and (B7):

$$H = \begin{bmatrix} \frac{p_x^2+p_y^2}{2m}+\hbar\omega_1 & \frac{\hbar g_A}{2}e^{i(\omega_A t+\phi_A)} & 0 \\ \frac{\hbar g_A}{2}e^{-i(\omega_A t+\phi_A)} & \frac{p_x^2+(p_y+\hbar k_A)^2}{2m}+\hbar\omega_2 & \frac{\hbar g_B}{2}e^{-i(\omega_B t+\phi_B)} \\ 0 & \frac{\hbar g_B}{2}e^{i(\omega_B t+\phi_B)} & \frac{p_x^2+(p_y+\hbar k_A+\hbar k_B)^2}{2m}+\hbar\omega_3 \end{bmatrix}. \quad \text{(B8)}$$

In order to remove the time dependence we apply some transformation Q [39] of the form

$$Q = \begin{bmatrix} e^{i(\theta_1 t+\phi_1)} & 0 & 0 \\ 0 & e^{i(\theta_2 t+\phi_2)} & 0 \\ 0 & 0 & e^{i(\theta_3 t+\phi_3)} \end{bmatrix}, \quad \text{(B9)}$$

so that the SE becomes

$$i\hbar\frac{\partial|\tilde{\Psi}\rangle}{\partial t} = \tilde{H}|\tilde{\Psi}\rangle, \quad \text{(B10)}$$

where $|\tilde{\Psi}\rangle = Q|\Psi\rangle$ and $\tilde{H} = QHQ^{-1} + i\hbar(\partial Q/\partial t)Q^{-1}$. The matrix representation is

$$\tilde{H} = \begin{bmatrix} \frac{p_x^2+p_y^2}{2m}+\hbar\omega_1-\hbar\theta_1 & \frac{\hbar g_A}{2}e^{i(\omega_A+\theta_1-\theta_2)t+i(\phi_A+\phi_1-\phi_2)} & 0 \\ \frac{\hbar g_A}{2}e^{-i(\omega_A+\theta_1-\theta_2)t-i(\phi_A+\phi_1-\phi_2)} & \frac{p_x^2+(p_y+\hbar k_A)^2}{2m}+\hbar\omega_2-\hbar\theta_2 & \frac{\hbar g_B}{2}e^{-i(\omega_B+\theta_3-\theta_2)t-i(\phi_B+\phi_3-\phi_2)} \\ 0 & \frac{\hbar g_B}{2}e^{i(\omega_B+\theta_3-\theta_2)t+i(\phi_B+\phi_3-\phi_2)} & \frac{p_x^2+(p_y+\hbar k_A+\hbar k_B)^2}{2m}+\hbar\omega_3-\hbar\theta_3 \end{bmatrix}. \quad \text{(B11)}$$

Choosing $\theta_1=-\omega_A$, $\theta_2=0$, $\theta_3=-\omega_B$, $\phi_1=-\phi_A$, $\phi_2=0$, and $\phi_3=-\phi_B$, Eq. (B11) becomes

$$\tilde{H} = \begin{bmatrix} E_1(p_x,p_y) + \hbar\omega_1 + \hbar\omega_A & \frac{\hbar g_A}{2} & 0 \\ \frac{\hbar g_A}{2} & E_2(p_x,p_y) + \hbar\omega_2 & \frac{\hbar g_B}{2} \\ 0 & \frac{\hbar g_B}{2} & E_3(p_x,p_y) + \hbar\omega_3 + \hbar\omega_B \end{bmatrix}, \tag{B12}$$

where we have taken

$$E_1(p_x,p_y) = \frac{p_x^2 + p_y^2}{2m}, \tag{B13a}$$

$$E_2(p_x,p_y) = \frac{p_x^2 + (p_y + \hbar k_A)^2}{2m}, \tag{B13b}$$

$$E_3(p_x,p_y) = \frac{p_x^2 + (p_y + \hbar k_A + \hbar k_B)^2}{2m}. \tag{B13c}$$

In order to further simplify the analysis, we set the zero energy at $E_1(p_{x0},p_{y0})+\hbar\omega_1+\hbar\omega_A$ for some specific momentum group with $p_x=p_{x0}$ and $p_y=p_{y0}$. Also, since ω_A and ω_B can be chosen independently, we can let $E_3(p_{x0},p_{y0})+\hbar\omega_3+\hbar\omega_B=E_1(p_{x0},p_{y0})+\hbar\omega_1+\hbar\omega_A$. With the energies thus set, Eq. (B12) becomes

$$\tilde{H} = \begin{bmatrix} 0 & \frac{\hbar g_A}{2} & 0 \\ \frac{\hbar g_A}{2} & -\delta & \frac{\hbar g_B}{2} \\ 0 & \frac{\hbar g_B}{2} & 0 \end{bmatrix}, \tag{B14}$$

where $\delta=[E_1(p_{x0},p_{y0})+\hbar\omega_1+\hbar\omega_A]-[E_2(p_{x0},p_{y0})+\hbar\omega_2]$. Using this Hamiltonian in Eq. (B10), we get the equations of motion as

$$\dot{\tilde{C}}_1(p_{x0},p_{y0},t) = -i\frac{g_A}{2}\tilde{C}_2(p_{x0},p_{y0}+\hbar k_A,t), \tag{B15a}$$

$$\dot{\tilde{C}}_2(p_{x0},p_{y0}+\hbar k_A,t) = -i\frac{g_A}{2}\tilde{C}_1(p_{x0},p_{y0},t) + i\delta\tilde{C}_2(p_{x0},p_{y0}+\hbar k_A,t) - i\frac{g_B}{2}\tilde{C}_3(p_{x0},p_{y0}+\hbar k_A+\hbar k_B,t), \tag{B15b}$$

$$\dot{\tilde{C}}_3(p_{x0},p_{y0}+\hbar k_A+\hbar k_B,t) = -i\frac{g_B}{2}\tilde{C}_2(p_{x0},p_y+\hbar k_A,t). \tag{B15c}$$

Assumption (5) allows us to make the adiabatic approximation so that we can set $\dot{\tilde{C}}_2(p_{x0},p_{y0},t)\approx 0$, and assumption (6) gives us $g_A=g_B=g_0$. Equations (B15) then simplify to

$$\dot{\tilde{C}}_1(p_{x0},p_{y0},t) = -i\frac{g_0^2}{4\delta}\tilde{C}_1(p_{x0},p_{y0},t) - i\frac{g_0^2}{4\delta}\tilde{C}_3(p_{x0},p_{y0}+\hbar k_A+\hbar k_B,t), \tag{B16a}$$

$$\dot{\tilde{C}}_3(p_{x0},p_{y0}+\hbar k_A+\hbar k_B,t) = -i\frac{g_0^2}{4\delta}\tilde{C}_1(p_{x0},p_{y0},t) - i\frac{g_0^2}{4\delta}\tilde{C}_3(p_{x0},p_{y0}+\hbar k_A+\hbar k_B,t), \tag{B16b}$$

where we have chosen to neglect state C_2 from here on due to the adiabatic approximation. We can now use another transformation on this system to make it more tractable. Let

$$\tilde{\tilde{C}}_1(p_{x0},p_{y0},t) = \tilde{C}_1(p_{x0},p_{y0},t)e^{i(g_0^2/4\delta)t}, \tag{B17a}$$

$$\tilde{\tilde{C}}_3(p_{x0},p_{y0}+\hbar k_A+\hbar k_B,t) = \tilde{C}_3(p_{x0},p_{y0}+\hbar k_A+\hbar k_B,t)e^{i(g_0^2/4\delta)t}. \tag{B17b}$$

The system in Eqs. (B16) then becomes

$$\dot{\tilde{\tilde{C}}}_1(p_{x0},p_{y0},t) = -i\frac{g_0^2}{4\delta}\tilde{\tilde{C}}_3(p_{x0},p_{y0}+\hbar k_A+\hbar k_B,t), \tag{B18a}$$

$$\dot{\tilde{\tilde{C}}}_3(p_{x0},p_{y0}+\hbar k_A+\hbar k_B,t) = -i\frac{g_0^2}{4\delta}\tilde{\tilde{C}}_1(p_{x0},p_{y0},t). \tag{B18b}$$

Solving this and reversing the transformations of Eqs. (B17) and (B9), we arrive at

$$C_1(p_{x0},p_{y0},t) = C_1(p_{x0},p_{y0},0)\cos\left(\frac{\Omega}{2}t\right) - ie^{i(\omega_A-\Omega/2)t+i\phi_A}\left[C_3(p_{x0},p_{y0}+\hbar k_A+\hbar k_B,0)e^{-i(\omega_B-\Omega/2)t-i\phi_B}\sin\left(\frac{\Omega}{2}t\right)\right], \tag{B19a}$$

$$C_3(p_{x0}, p_{y0} + \hbar k_A + \hbar k_B, t) = -ie^{i(\omega_B - \Omega/2)t + i\phi_B} \times \left[C_1(p_{x0}, p_{y0}, 0) e^{-i(\omega_A - \Omega/2)t - i\phi_A} \sin\left(\frac{\Omega}{2}t\right) \right] + C_3(p_{x0}, p_{y0} + \hbar k_A + \hbar k_B, 0) \cos\left(\frac{\Omega}{2}t\right), \quad \text{(B19b)}$$

where we let $\Omega = g_0^2/2\delta$. It should be noted, however, that these solutions were arrived at only for the specific momentum group where $p_x = p_{x0}$ and $p_y = p_{y0}$. This was the case where both laser fields were equally far detuned. Other momentum groups will have slightly different solutions due to the Doppler shift, which causes the detunings to be perturbed. For a more accurate description, we need to numerically solve each momentum group's original three equations of motion without making any approximations. This is what we do in our computational model. For a basic phenomenological understanding of the interferometer, however, it is sufficient to assume that the above analytical solution is accurate for all momentum components.

[1] *Handbook of Micro-lithography, Micromachining and Microfabrication*, edited by P. Rai-Choudhury, SPIE Press, Bellingham, WA (1979).
[2] *Microlithography Science and Technology*, edited by J. R. Sheats and Bruce W. Smith (Marcel Dekker, New York, 1997) Chap. 7.
[3] Joseph W. Goodman, *Introduction To Fourier Optics* (McGraw-Hill, New York, 1996).
[4] M. H. Anderson *et al.*, Science **269**, 198 (1995).
[5] K. B. Davis *et al.*, Phys. Rev. Lett. **75**, 3969 (1995).
[6] C. J. Borde, Phys. Lett. A **140**, 10 (1989).
[7] M. Kasevich and S. Chu, Phys. Rev. Lett. **67**, 181 (1991).
[8] L. Gustavson, P. Bouyer, and M. A. Kasevich, Phys. Rev. Lett. **78**, 2046 (1997).
[9] M. J. Snadden, J. M. McGuirk, P. Bouyer, K. G. Haritos, and M. A. Kasevich, Phys. Rev. Lett. **81**, 971 (1998).
[10] J. M. McGuirk, M. J. Snadden, and M. A. Kasevich, Phys. Rev. Lett. **85**, 4498 (2000).
[11] Y. Tan, J. Morzinski, A. V. Turukhin, P. S. Bhatia, and M. S. Shahriar, Opt. Commun. **206**, 141 (2002).
[12] D. Keith, C. Ekstrom, Q. Turchette, and D. E. Pritchard, Phys. Rev. Lett. **66**, 2693 (1991).
[13] J. H. Thywissen and M. Prentiss, e-print physics/0209084.
[14] B. Brezger *et al.*, Europhys. Lett. **46**, 148 (1999).
[15] R. Stützle *et al.*, J. Opt. B: Quantum Semiclassical Opt. **5**, S164 (2003).
[16] D. S. Weiss, B. C. Young, and S. Chu, Phys. Rev. Lett. **70**, 2706 (1993).
[17] T. Pfau *et al.*, Phys. Rev. Lett. **71**, 3427 (1993).
[18] U. Janicke and M. Wilkens, Phys. Rev. A **50**, 3265 (1994).
[19] R. Grimm, J. Soding and Yu. B. Ovchinnikov, Opt. Lett. **19**, 658 (1994).
[20] T. Pfau, C. S. Adams, and J. Mlynek, Europhys. Lett. **21**, 439 (1993).
[21] K. Johnson, A. Chu, T. W. Lynn, K. Berggren, M. S. Shahriar, and M. G. Prentiss, Opt. Lett. **20**, 1310 (1995).
[22] M. S. Shahriar, Y. Tan, M. Jheeta, J. Morzinsky, P. R. Hemmer, and P. Pradhan, e-print quant-ph/0311163; J. Opt. Soc. Am. B (2005) (in press).
[23] B. E. A. Saleh and M. C. Teich, *Fundamentals of Photonics* (Wiley-Interscience, New York, 1991).
[24] L. Dobrek *et al.*, Phys. Rev. A **60**, R3381 (1999).
[25] J. Denschlag *et al.*, Science **287**, 97 (2000).
[26] S. Swain, J. Phys. B **15**, 3405 (1982).
[27] M. Prentiss, N. Bigelow, M. S. Shahriar, and P. Hemmer, Opt. Lett. **16**, 1695 (1991).
[28] P. R. Hemmer, M. S. Shahriar, M. Prentiss, D. Katz, K. Berggren, J. Mervis, and N. Bigelow, Phys. Rev. Lett. **68**, 3148 (1992).
[29] M. S. Shahriar and P. Hemmer, Phys. Rev. Lett. **65**, 1865 (1990).
[30] M. S. Shahriar, P. Hemmer, D. P. Katz, A. Lee, and M. Prentiss, Phys. Rev. A **55**, 2272 (1997).
[31] P. Meystre, *Atom Optics* (Springer Verlag, Berlin, 2001).
[32] *Atom Interferometry*, edited by P. Berman (Academic Press, New York, 1997).
[33] *Fiber Optic Rotation Sensors*, edited by S. Ezekiel and A. Arditty (Springer-Verlag, Berlin, 1982).
[34] J. McKeever *et al.*, Phys. Rev. Lett. **90**, 133602 (2003).
[35] S. J. van Enk *et al.*, Phys. Rev. A **64**, 013407 (2001).
[36] A. C. Doherty *et al.*, Phys. Rev. A **63**, 013401 (2001).
[37] K. K. Berggren *et al.*, Science **269**, 1255 (1995).
[38] S. B. Hill *et al.*, Appl. Phys. Lett. **74**, 2239 (1999).
[39] M. S. Shahriar, M. Jheeta, Y. Tan, P. Pradhan, and A. Gangat, Opt. Commun. **243**, 183 (2004).
[40] A. Corney, *Atomic and Laser Spectroscopy* (Oxford Science, Oxford, 1976).
[41] M. R. Andrews *et al.*, Science **275**, 637 (1997).
[42] Y. Torii *et al.*, Phys. Rev. A **61**, 041602 (2000).
[43] A. Marte, T. Volz, J. Schuster, S. Dürr, G. Rempe, E. G. M. van Kempen, and B. J. Verhaa, Phys. Rev. Lett. **89**, 283202 (2002).
[44] T. Volz, S. Dürr, S. Ernst, A. Marte, and G. Rempe, Phys. Rev. A **68**, 010702(R) (2003).
[45] L. Allen and J. H. Eberly, *Optical Resonance and Two-Level Atoms* (Dover, New York, 1974).